Efficiency and Stability enhancement in Perovskite Solar Cells by inserting Lithium-Neutralized Graphene Oxide as Electron-Transporting Layer.

Antonio Agresti, Sara Pescetelli, Lucio Cinà, Dimitrios Konios, George Kakavelakis, Emmanuel Kymakis, and Aldo Di Carlo[*]

Antonio Agresti, Sara Pescetelli, A. Di Carlo,
CHOSE (Centre for Hybrid and Organic Solar Energy), Department of Electronic Engineering, University of Rome Tor Vergata, via del Politecnico 1, 00133 Rome, Italy
E-mail: aldo.dicarlo@uniroma2.it

Dimitrios Konios, George Kakavelakis, Emmanuel Kymakis
Center of Materials Technology and Photonics & Electrical Engineering Department, School of Applied Technology, Technological Educational Institute (T.E.I) of Crete, Heraklion, 71 004, Crete, Greece

This work proposes a new perovskite solar cell structure by including Lithium-Neutralized Graphene Oxide (GO-Li) as the electron transporting layer on top of the mesoporous TiO_2 (m-TiO_2) substrate. The modified work-function of GO after the intercalation of Li atoms (4.3eV) exhibits a good energy matching with the TiO_2 conduction band, leading to a significant enhancement of the electron injection from the perovskite to the m-TiO_2. The resulting devices exhibit an improved short circuit current and fill factor and a reduced hysteresis. Furthermore the GO-Li electron transporting layer (ETL) partially passivates the oxygen vacancies/defects of m-TiO_2 by resulting in an enhanced stability under prolonged 1 SUN irradiation.

1. Introduction

Semiconducting perovskite materials based on organoleadtrihalide compounds are promising solution-process light harvesters. Over the past few years, perovskite solar cells (PSC) have

experienced a tremendous interest, moving from a power conversion efficiency (PCE) of 9.7% [1] up to 20.1 %.[2] This phenomena is mainly due to the peculiar properties of the perovskite material which combine a high absorption coefficient with a decent mobility of charge carriers.[1,3] This permits the utilization of an ultrathin absorber layer[4–8] leading to a very high PCE.

To reach the theoretically predicted PCE maximum is necessary to find an optimal trade-off between high optical absorption and extremely thin absorbers. In fact, while it has been possible to reach high experimental values of short circuit current density (Jsc) and open circuit voltage (Voc), consistent with the theoretical values,[9] further work is needed to increase the fill factor (FF) that today remains the bottleneck for the PCE enhancement. In this context, the optimization of interfaces between absorber, carrier transport layers, and electrode contact layers is crucial for an efficient carrier transport. Thus to improve the PCE of the PSCs three main aspects need to be taken into consideration: the band alignment, the interface structure and its passivation.[9]

Furthermore, it must be taken into account that the injection times of electrons and holes in PSCs have been measured to be 0.4 and 0.6 ns, respectively, which are still orders of magnitude longer than the hot carrier cooling (or thermalization) time (~0.4 ps).[10] Thus, a large amount of the converted photon energy is wasted in the thermalization process and in the carrier trapping. In this context, several materials have been proposed to facilitate electron/hole extractions, including fullerene,[11] graphene,[12] or core/shell metal nanoparticles.[13] Although graphene based materials have been demonstrated to improve the performance and stability of organic and hybrid photovoltaic devices as recently reviewed by E. Singh and H. S. Nalwa [14][15], a direct evidence is yet to be obtained regarding their role as a fast electron injector rather than just an electron trapping center.[16]

In this work, to improve the electron extraction from the perovskite absorber into the mesoporous TiO_2, we used an additional lithium-neutralized graphene oxide (GO-Li) layer as electron-transporting Layer. GO-Li has been already used as ETL in organic photovoltaic devices by G. Kakavelakis et al..[17] The authors demonstrated that the replacement of -H in the carboxyl groups of GO by Li atoms can effectively reduce the working function (WF) of GO from 4.9 to 4.3 ± 0.1 eV. Due to the low electronegativity and low WF, Li atoms lose their valence electrons to the GO plane, and the resulting positive Li^+ induces dipoles. This transfer of charge from the metal to the GO leads to a shift in the Fermi level toward the vacuum and a consequent decrease in WF.[18]

Since the WF of GO-Li displays a good match with the LUMO level of mesoporous TiO_2, in this work we propose a new efficient perovskite solar cell structure by including the GO-Li as an interlayer between the TiO_2 and the perovskite harvester. The resulting PSCs exhibit enhanced J_{SC} and FF and reduced hysteresis with respect to control devices without the GO-Li ETL. The reported analysis points out the beneficial effects of GO-Li layer on both device electrical performance and long-term stability. In particular the deep analysis of both 1 SUN and in dark current-voltage (I-V) characteristics, transient measurements and steady state fluorescence spectroscopy reveal an improved charge extraction/injection at the cell photo-electrode (PE) when GO-Li is used as ETL. At the same time GO-Li layer is demonstrated to passivate the oxygen defects/vacancies in the mesoporous TiO_2 layer that act as a reactive centers when the device is exposed to the moisture attack. That results in an improved stability and in an enlarged device lifetime of the not-encapsulated devices employing GO-Li as ETL, under 1 SUN prolonged stress test.

2. Results and discussion

Two sets (8 cells per type) of PSC structures were fabricated and compared, namely reference

PSCs composed by FTO/c-TiO$_2$/m-TiO$_2$/perovskite/Spiro-MeOTAD/Au and PSCs fabricated

with GO-Li as ETL onto m-TiO$_2$ layer [FTO/c-TiO$_2$/m-TiO$_2$/GO-Li/perovskite/Spiro-

MeOTAD/Au] as reported in **Figure 1A** and 1B, respectively.
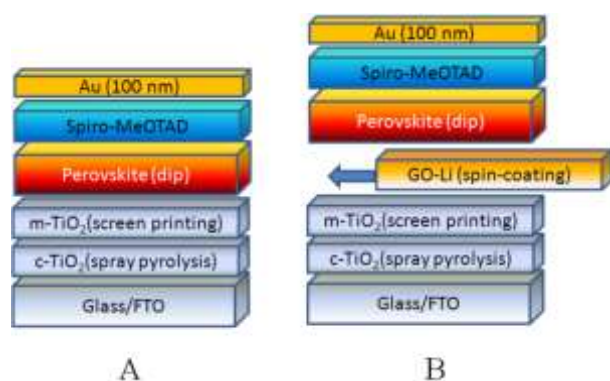
Figure 1. Structures of tested devices, without GO-Li layer (A) as reference and with GO-Li layer (B) on m-TiO$_2$.

The GO-Li chemical and physical properties were widely discussed in a previous work[17] and

have been used as starting point to motivate the position of the GO-Li ETL in the device

architecture. In fact the UPS measurement exhibited an error of ±0.05 eV, providing a WF of

4.27±0.05 eV for GO-Li [17], which perfectly match the TiO$_2$ conduction band as

schematically showed in the energy band diagram reported in Figure 2. The maximum WF

value of GO-Li required to inject electrons into the m-TiO$_2$ layer without any energy barrier

should be 4.25 eV (k$_B$T~0.025 eV at RT), which is in the range of the measured with UPS

GO-Li WF values.
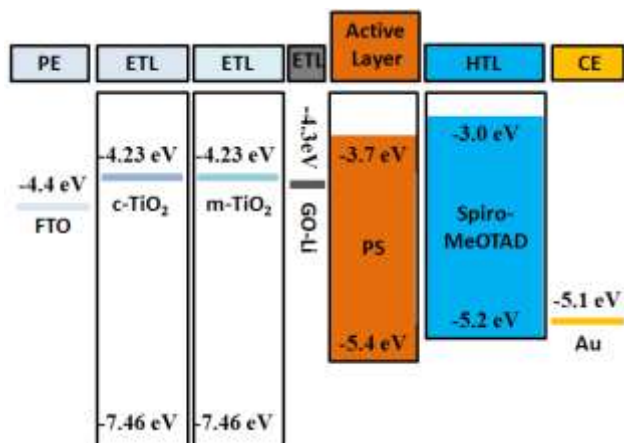
Figure 2. Schematic energy band diagram of different functional layers in perovskite solar cell relative to vacuum. The band alignments are not to scale and show only the relative positions.

The TiO_2 energy band diagram has been extracted by Ref..[19,20] The anatase crystal form of both c-TiO2/m-TiO2 and c-TiO2/m-TiO2/GO-Li substrates was verified by mean of resonance Raman spectroscopy (Figure S1).[21–23] That in combination with the absorbance measurements (Figure S2) ensure a band gap of about 3.2 eV[24] for both the analyzed substrates.

The presence of typical D (Disorder) and G (Graphitic) vibrational bands of GO [25–27] in the Raman spectrum of c-TiO2/m-TiO2/GO-Li carried out by focusing the laser beam onto the m-TiO2 layer confirms the interpenetration of GO-Li in the mesoporous layer.

Perovskite and doped spiro-MeOTAD energy levels were extracted by the recent work of Schulz and co-authors[28] reporting an energy gap of 3.7 eV for $CH_3NH_3PbI_3$ perovskite and a highest occupied molecular orbital (HOMO) level of 5 eV for doped spiro-MeOTAD layer. The current density and voltage (J-V) characteristics of the best performing PSCs at 1 SUN illumination and without encapsulation are reported in Figure 3, while the extracted electrical parameters are reported in Table.1. The results repeatability is checked on 8 realized devices per typology; the related electrical parameters and the standard deviation are reported in Figure S3.

WILEY-VCH
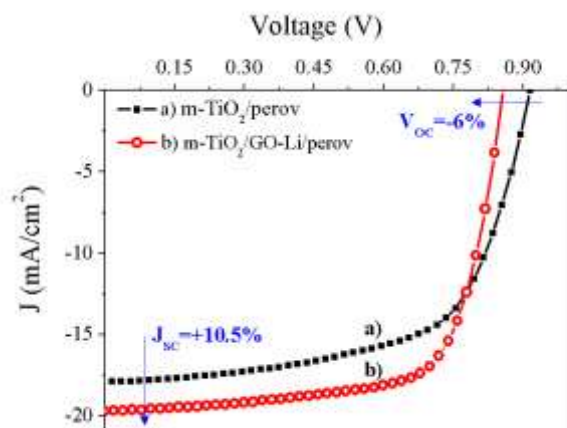
Figure 3. J-V curves of best performing devices without encapsulation and under 1 SUN illumination condition. The GO-Li based cell (curve b) showed an increased J_{SC} (+10.5%) and a sligtly reduced V_{OC} (-6%) when compared with the reference one (curve a) leading to an increased efficiency (+12%).

Table.1. Electrical parameters of the best device extracted by the J-V characteristics reported in Figure 3. Last column reports the average efficiency of both PSC sets. The electrical parameters and the related standard deviation for all the tested devices are reported in Figure S3.

Samples	V_{OC} [V]	J_{SC} [mA/cm^2]	Fill Factor [%]	Efficiency [%]	Average PCE
reference	0.915	-17.7	65.4	10.3	9.66
GO-Li	0.859	-19.61	70.3	11.8	11.14

Notably the best device comprising GO-Li layer showed a remarkable improvement in PCE

(+12%) as compared with the performance of the reference sample. In particular the PCE

improvement can be related to an increase of J_{SC} (+10.5%) and the FF (+7.5%) while the V_{OC}

undergoes a slight decrease (-6%). The small V_{OC} change is consistent with the fact that the

main role of the ultrathin GO-Li layer is to facilitate the electron injection into the TiO$_2$

layer.[14] Moreover, the addition of free lithium ions into the electrolyte solution of Dye

Sensitized Solar Cells (DSC's) is well known to insert more deep surface states below the

TiO$_2$ conduction band (CB) edge.[29] The adsorption of lithium cations onto the mesoporous

TiO$_2$ surface leads to a downward displace of TiO$_2$ CB that adversely affects the V_{OC}. Thus, it

is reasonable to expect a similar m-TiO$_2$ CB downshift effect upon the addition of the GO-Li

interlayer, resulting in a lowering of the devices V_{OC}. The repeatability of the results has been proved by testing 8 devices for each type of PSC. An average PCE improvement of about 12% was found also for the PSC set with GO-Li ETL.

In order to explain why the GO-Li insertion is beneficial for the devices performance and in particular for the J_{SC}, a series of electro-optical measurements have been carried out onto the non-encapsulated devices. Figure 4 shows the incident photon-to-current conversion efficiency (IPCE) spectra in the visible wavelength region (from 300 nm to 800 nm) for both the investigated devices. The reported integrated photocurrent density of IPCE spectra exhibit values which are in agreement (percentage difference of 0.98% and 2.6% for best performing GO-Li based and reference devices respectively) with the corresponding values measured under sun simulator. It is worth to note that the overall IPCE improvement is localized in the long wavelength spectral region, between 500 and 780 nm. Since the absorption of GO-Li thin layer is expected to be small, the IPCE enhancement can likely stem from a better injection of electrons generated by long-wavelength part of the excitation spectrum. In fact, the longer wavelength region corresponds to the low energy photogenerated electrons that could be easy trapped into the perovskite layer prior to be injected into the TiO_2 layer. Thus, the insertion of GO-Li aids the electron extraction at the TiO_2/perovskite interface by improving the integrated photocurrent density.
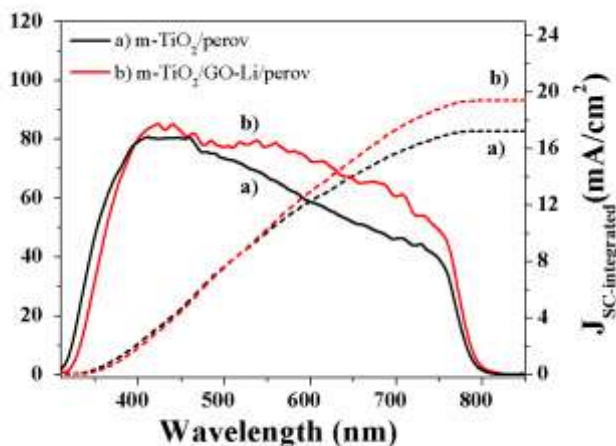
Figure 4. IPCE spectrum of GO-Li based (curve b, continuous line) and reference (curve a, continuous line) perovskite solar cells without encapsulation. The righthand axis indicates the integrated photocurrent that is expected to be generated under AM1.5G irradiation for GO-Li based (curve b, dashed line) and reference structure (curve a, dashed line).

To further support this observation, steady state fluorescence measurement on photoelectrodes (PEs) fabricated with and without the GO-Li layer have been performed (Figure 5). Under the same experimental condition, the FTO/TiO$_2$/perovskite and FTO/TiO$_2$/GO-Li/perovskite samples demonstrate a photoluminescence (PL) emission at 760 nm which is typical of the perovskite layer. Notably, when GO-Li is inserted in the PE the perovskite PL is dramatically quenched (by nearly 55%). Since the PL emission stems from the radiative recombination in perovskite layer, a reduced emission is symptomatic of an enhanced electron injection in the TiO$_2$ layer, further confirming the role of GO-Li layer in enhancing the electron extraction.
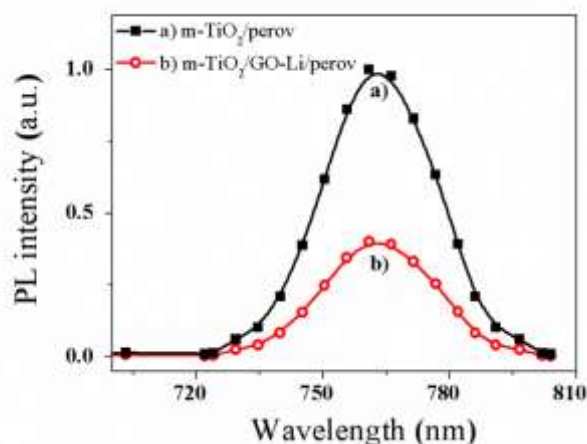
Figure 5. Photoluminescence emission spectra of FTO/c-TiO$_2$/m-TiO$_2$/perovskite (curve a) and FTO/c-TiO$_2$/m-TiO$_2$/GO-Li/perovskite (curve b) substrates before the HTM deposition. The excitation wavelenght has been set at 410nm.

GO-Li passivation effect of m-TiO$_2$ surface cannot, however, be immediately excluded. First of all the passivation effect of GO-Li onto the m-TiO$_2$ oxygen vacancies can be clearly detected by applying Raman spectroscopy on the glass-FTO/c-TiO$_2$/m-TiO$_2$ substrate before (curve a Fig.S2) and after (curve b Fig.S2) the deposition of the GO-Li layer. In fact the presence of oxygen vacancies results in a broadening of the typical anatase TiO$_2$ vibrational bands due to a degradation of crystallinity and in a shift of the main E$_{g(1)}$ band (145 cm^{-1}) towards higher wavenumbers.[30] The shift from 149 cm^{-1} to 145 cm^{-1} and the decreased linewidth (FWHM) of the E$_{g(1)}$ mode after the intercalation of GO-Li layer onto the m-TiO$_2$ detailed in tab. S1 give a clear evidence of the oxygen vacancies passivation effect by GO-Li insertion. Furthermore in a complete device TiO$_2$ defect passivation could reduce the trap assisted recombination during the charge extraction at the negative electrode, by further enhancing the J$_{SC}$. At this purpose, dark I-V and transient measurements have been carried out by employing the ARKEO setup described in the experimental section. The in dark I-V measurement provides useful information about the recombination processes occurring in the devices.[31] In fact, when the diode model is employed to fit the in dark I-V curve the ideality factor *n* can be easily extracted. In absence of recombination *n* should be equal to the unity whereas trap-assisted recombination can change it up to 2.[32,33] Figure 6 shows the in dark I-V curves for the best PSCs with and without GO-Li, together with the series resistance (Rs) and *n* factor values extracted by the non-linear curve-fitting procedure.

9
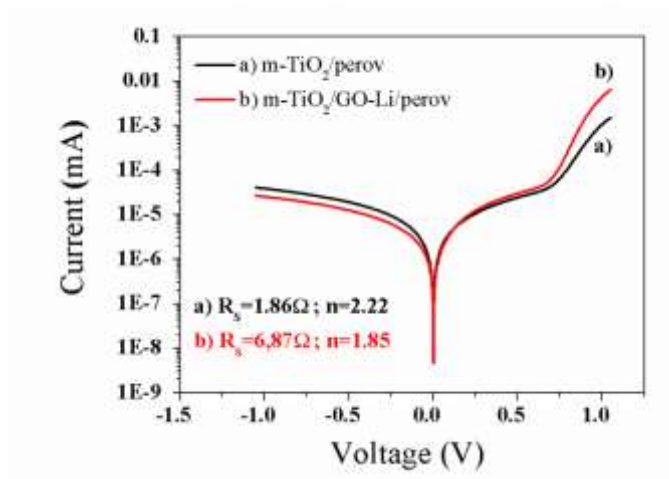
Figure 6. The reported series resistance (R$_S$) and diode ideality factor (*n*) are extracted by the diode model fitting performed for the positive voltage values.

The raw data and the fitted curves for both reference and GO-Li based samples are plotted in Figure S4 (panel A and B respectively) for the voltage value between 0.1 and 1 V where the fitting has been performed. As expected for perovskite based solar cell, *n* extracted values are significantly larger than 1 for both tested devices, demonstrating that trap assisted recombination plays a substantial role in the recombination process.[34] However, PSC with the GO-Li ETL showed an *n* factor and a R$_S$ smaller with respect to the reference PSC, suggesting a decreased density of trap state at TiO$_2$/perovskite interface when Go-Li is added. Mesoporous TiO$_2$ is well known to contain many oxygen vacancies, in particular at the surface[35,36] by generating electrons trap sites at approximately 1 eV below the conduction band edge.[37] Thus a not negligible fraction of the electrons injected into TiO$_2$ are trapped on these sites an can recombine with holes in the spiro-OMeTAD.[38] On the contrary, when TiO$_2$ is treated with GO-Li, the residual oxygen moiety of GO will passivate the TiO$_2$ layer enhancing photocatalytic properties because of the increase in the transport efficiency of the photogenerated electrons.[39]

The capability of GO-Li to reduce trap assisted recombination is finally demonstrated by a remarkable decrease in the J-V curve hysteresis. Figure 7 shows the forward and reverse J-V

scans for both tested devices, by reporting the hysteresis index calculated as defined by Sanchez et al..[40] As evident, both tested devices presented a marked hysteric behaviour but, notably, the insertion of GO-Li in the cell structure reduces the hysteresis factor by 50%. The origin of hysteresis phenomenon in perovskite solar cell is nowadays not completely understood but several explanation have been proposed and supported by theoretical studies.[41] In particular the hysteresis phenomenon is suspected to be related to the perovskite interface properties.[40,42] Very recently Reenen and co-worker[43] modelled the hysteric behaviour by including ion migration phenomena and electronic charge traps, by finally achieving a good agreement with the experimental data. The authors demonstrated that trapped electronic charges recombine with oppositely charged free electronic carriers, with their density to be depended on the bias-dependent ion distribution in the perovskite. In this context, the ions movement inside the perovskite layer strongly depends on the structural properties of the sensitizer, while the carrier trapping efficiency is related to the effective presence of deep trap states in particular at the perovskite/transporting layer interface. Thus, we can confidently postulate that the passivation effect of GO-Li onto the TiO_2 traps can consistently reduce the amount of trapped electrons by reducing the hysteresis index.
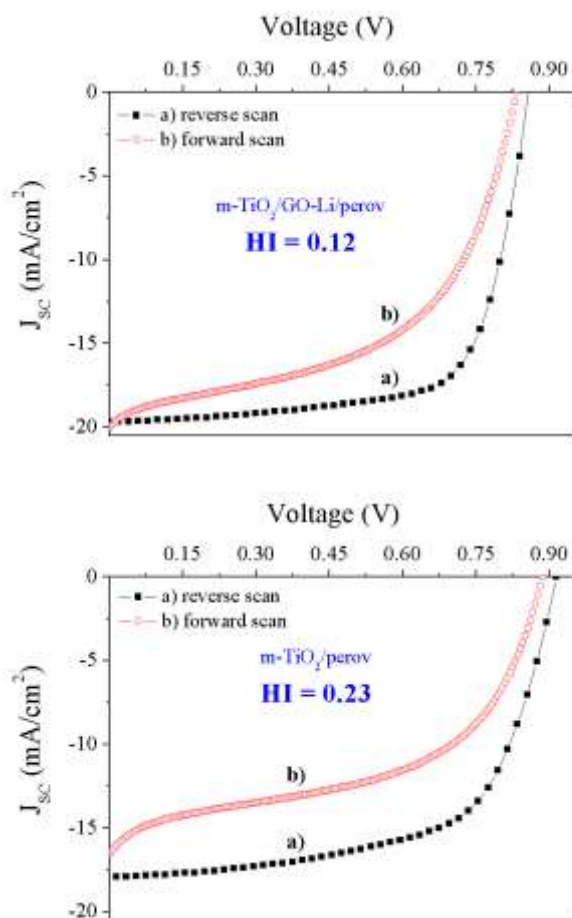
Figure 7. J−V curves measured at forward scan (curve b) and reverse scan (curve a) for the best performing tested devices: Go-Li based sample (panel A) and reference sample (panel B). The hysteresis index (HI) calculated in accordarce with ref.[42] are reported in each panel.

To finally conclude the analysis of the recombination phenomena, open circuit photovoltage decay (OCVD) measurements under large perturbation regime have been carried out. The debate on the transient measurement interpretation for perovskite solar cell is still open. A commonly accepted conclusion is that the response time derived from OCVD measurement cannot be generally interpreted as a recombination lifetime because other types of relaxation behaviour influence the decay of the photovoltage.[40] In our case tested devices showed a very similar V_{OC} exponential decay (Figure 8). However by extracting the average time decay constant (provided by a bi-exponential fitting[44] of the V_{OC} decay) the GO-Li based samples showed a slightly decreased time consistent with the decreased V_{OC} under 1 SUN illumination

(Figure 3) and even with the increased recombination current at 1V under dark condition

(Figure 6). The slightly faster decay time constant τ_b extracted in the case of GO-Li based

samples confirms that the unfavourable m-TiO$_2$ CB downshift due to the GO-Li presence

overwhelms the advantageous passivation effects of TiO$_2$ oxygen vacancies. This confirms

that the GO-Li enhancement effect is mainly attributed to improved charge injection at the

electrode and not to decreased charge recombination efficiency.
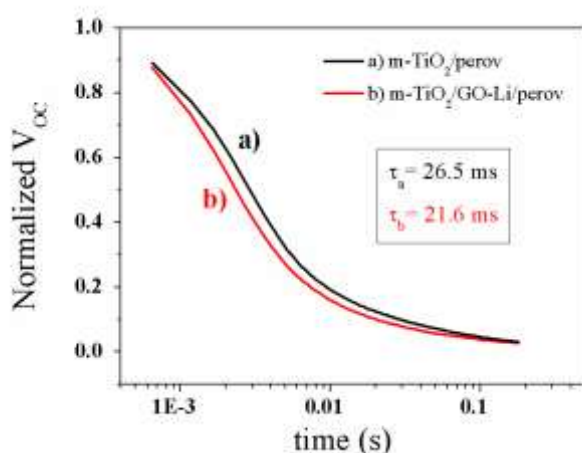
Figure 8. Open Circuit Photovoltage Decay (OCVD) profiles for the best performing tested
devices, GO-Li based (curve b) and reference device (curve a) in semi-logarithmic scale . The
averaged decay constant time (τ) is reported for each device and is calculated as weight
average of time constants extracted by the bi-exponential fit for each OCVD profile.

In order to finally confirm the remarkable improvement of the charge extraction in GO-Li

PSCs, the J_{SC} of both investigated devices has been recorded by progressively increasing the

irradiation level (P_{inc}) up to 0.18 mW/cm^2. J. You and co-workers[45] employed this method to

detect the presence of energy barrier in perovskite devices. In fact, a quite non-linear trend of

J_{SC} versus light intensity is indicating the presence in the device of energy barriers affecting

the charge extraction process. Figure 9 shows the J_{SC} vs. P_{inc} for both the best performing

devices (curve a and b for device without and with GO-Li respectively) and the R^2 parameter

extracted for both linear fitted curves. Notably the use GO-Li as ETL improves the R^2 of

fitted curve, by showing a more linear trend of J_{SC}-P_{inc} curve when compared with reference sample.
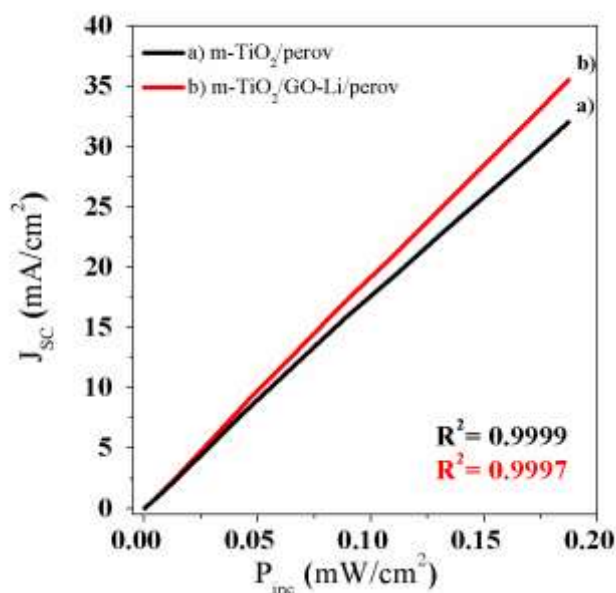
Figure 9. Variation of density of short circuit current (J_{SC}), versus incident ligtht power (P_{inc}) fitted by a linear relationship. The reported coefficient of determination (R^2) indicates the goodness of the linear fit.

Thus it is possible to finally conclude that the insertion of GO-Li as interlayer ETL in perovskite solar cell has the effect to boost the overall efficiency by enhancing both the device's J_{SC} and the FF. In fact, the GO-Li insertion has been demonstrated to improve the electron extraction at the PE by retaining a good balance between holes and electrons extraction at the PE. On the contrary the V_{OC} value undergoes an overall decrease due to the downward shift of m-TiO$_2$ CB only partially balanced by the passivation of TiO$_2$ surface defect. Nevertheless the losing in V_{OC} is largely compensated by the increase in J_{SC} finally leading to an increased efficiency.

Finally, we investigated the stability of tested device under prolonged illumination condition (100 mW/cm^2) provided by a white LED at room temperature, as described in the experimental section. J-V curves, in both reverse and forward scan direction, were acquired

every 6 minutes during the aging time and electrical parameters were extracted for each J-V

curve. Dark J-V characteristics, OCVD transient analysis and the light dependent

measurements (J_{SC} vs. light incident power) were recorded at the beginning and at the end of

the stress test. Cells were not encapsulated.

The degradation trends of normalized electrical parameters are reported in Figure 10.
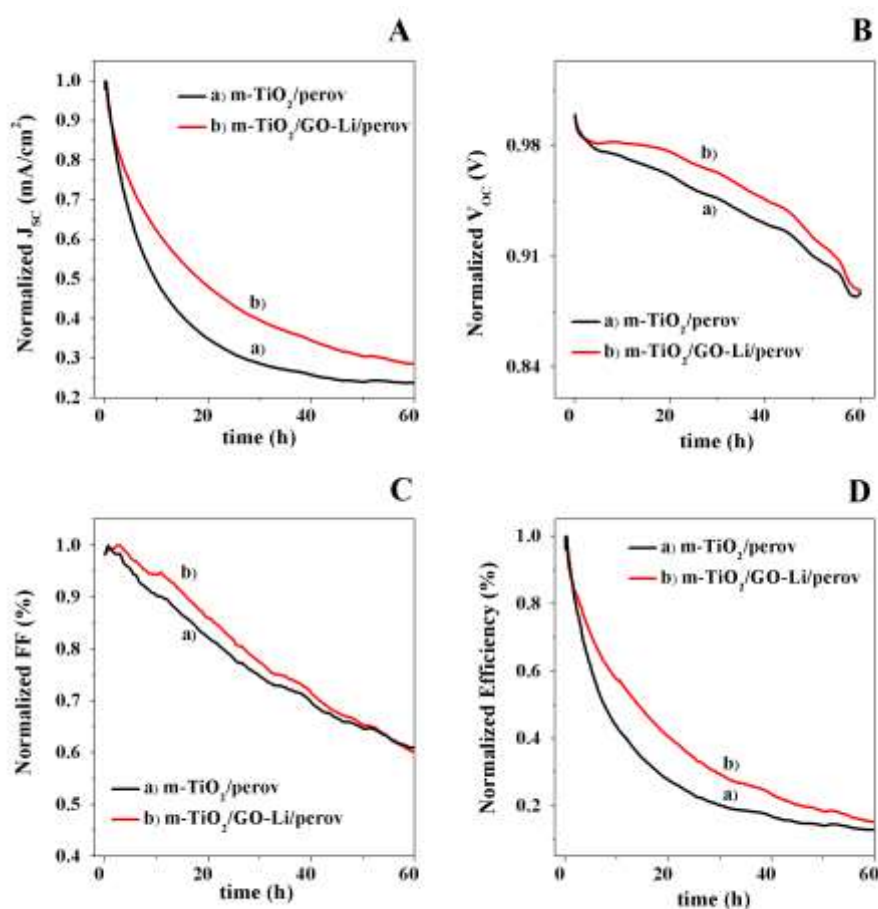
Figure 10. Comparison of the stability for not encapsulated GO-Li based (curves b) and reference devices (curves a) tested under 1 SUN illumination condition provied by a white LED and room temperature. In particular panel A, B, C, D shows the J_{SC}, V_{OC}, FF and η degradation during the first 60 hours of aging test.

The efficiency decrease is mainly determined by losses in J_{SC} (Figure 10A) and FF (Figure

10C) for both tested devices but with different degradation rates. Surprisingly, the device with

GO-Li ETL shows an improved stability under the prolonged light soaking test than the

reference device. The same results have been obtained by examining the electrical parameters trends extracted by the forward scan J-V characteristics (here not reported).

These results clearly show the use of GO-Li ETL as an effective pathway towards the improvement of the perovskite solar cell stability, even though further investigations are needed to clarify the effective role of GO-Li in slowing down the degradation processes. The main degradation phenomenon for PSC involves the doped spiro-MeOTAD and the perovskite active layers. As recently reported in our previous work[46] the replacement of doped spiro-MeOTAD with organic hole conductor layer such as phthalocyanine derivative could improve the devices stability. In fact spiro-MeOTAD, in its pristine form, suffers from low hole mobility and low conductivity and dopants are needed to improve this effect. Usually tert-butylpyridine (TBP) is added to the spiro-MeOTAD solution to obtain a significant improvement in the V_{OC} while and Lithium Bis (Trifluoromethanesulfonyl)Imide (LiTFSI) is added to improve the J_{SC}[47]. These additives are well known to reduce the device's stability. Hawash and co-workers[48] demonstrated the diffusion of the dopant upon air and light exposure causes the slowing down of hole mobility and finally degrades the perovskite active layer. Thus, most likely the degrading process involves both the HTM and the sensitizer by gradually slowing down the hole collection efficiency of HTL and the generation of free charges in the perovskite active layer.

Leijtens and co-workers[38] proposed a detailed degradation mechanism arising from light-induced desorption of surface-adsorbed oxygen. In fact, due to the presence of TiO_2 oxygen vacancies, oxygen radical can be adsorbed on TiO_2 surface and reacts with the photogenerated holes in TiO_2 layer. The oxygen is thus released by leaving a deep electron trap state; the consequently trapped electron can recombine with the excess of holes in the doped-hole transporter. This phenomenon is supposed to accelerate during the aging test that cause radical oxygen adsorption/release at TiO_2 vacancies and a slowing down of hole mobility in

WILEY-VCH

the HTL due to the abovementioned spiro-MeOTAD degradation. Consequently, our results strongly suggest that the TiO_2 traps are passivated by the GO-Li ETL enhancing the stability of the PSCs.

3. Conclusions

This work reports a new efficient ETL for PSCs. In particular GO-Li has been inserted in a typical device structure between the sensitizer and m-TiO_2 layer. Electrical, optical and transient analysis demonstrated the main effect of GO-Li in improving the electron injection from the sensitizer to the m-TiO_2 layer by remarkably increasing the J_{SC} (+10.5%). Furthermore the good balance between electrons and holes extraction at the electrodes resulted in an increased FF (+7.5%) while a better injection of electrons generated by long-wavelength part of the excitation spectrum results in a broadened IPCE spectrum. Moreover, a reduction of about 50% in devices J-V curves hysteresis demonstrated the capability of GO-Li layer to reduce trap assisted recombination at m-TiO_2/perovskite interface. Notably the tested devices showed an improved stability when subjected, without encapsulation, to prolonged illumination aging test. The physical mechanism for an increased stability of GO-Li based device is yet under investigation. Nevertheless the reported analysis suggests that the enhanced device's stability stems mainly from the passivation of m-TiO_2 oxygen vacancies that are the main reaction centers for moisture attack. The relevant results underline how the utilization of a facile WF tuning of graphene based material can provide optimized efficiency and improve the life-time of PSCs. Furthermore, the innovative application of GO-Li in organoleadtrihalide PSCs together with the employed vacuum and vapor assisted technique open a viable route to improve further the stability of the device by retaining this technology repeatable and suitable for next large area applications.

4. Experimental section

4.1. Material

4.1.1. Preparation of Graphene Oxide (GO)

GO was prepared from graphite powder (Alfa Aesar. ~200 mesh) according to a modified Hummers' method.[49] In more detail, graphite powder (1.0 g) was placed into a mixture of H_2SO_4 (23 mL, 98%) and $NaNO_3$ (0.5 g). The mixture was then stirred and cooled in an ice bath. While maintaining vigorous stirring, $KMnO_4$ (3.0 g) was then added in portions over a period of 2 h. The reaction mixture was left for 4 h in order to reach room temperature before being heated to 35 °C for 30 min. It was then poured into a flask containing deionized water (50 mL) and further heated to 70 °C for 15 min. The mixture was then decanted into 250 mL of deionized water and the unreacted $KMnO_4$ was removed by adding 3% H_2O_2. The reaction mixture was then allowed to settle and decanted. The graphite oxide obtained was then purified by repeated centrifugation and re-dispersed in deionized water until a negative reaction on sulphate ion (with $Ba(NO_3)_2$) was achieved. Finally, the resulting GO was dried at 60 °C in a vacuum oven for 48 h before use.

4.1.2 Preparation of Graphene Oxide functionalized with Lithium (GO-Li)

The chemical functionalization of GO with lithium was performed using an aqueous solution of the previous prepared GO (1.5 mg mL^{-1}, 40 mL). Li_2CO_3 (200 mg) was then added and the solution was stirred for 1 h. PVDF membrane (0.45 μm) was used to filter and collect the solid, which was then dissolved in water (20 mL). The process of dissolution and filtration was repeated two times. The prepared GO-Li was dissolved in water:ethanol (1:3).[50]

4.2 Perovskite solar cells realization

Solar cells with an active area of 0.1 cm^2 were prepared on Fluorine-doped Tin Oxide (FTO) conductive glass (Pilkington, 8 Ω/□, 25mm x 25mm) patterned through raster scanning laser (λ=1064nm, Nd:YVO$_4$ pulsed at 30 kHz, average output power P=10 W). The patterned

substrates were cleaned in an ultrasonic bath, using detergent with de-ionized water, acetone and 2-propanol (10 min for each step). A patterned compact TiO_2 (c-TiO_2) layer was deposited onto the patterned FTO by Spray Pyrolysis Deposition (SPD). To measure the final thickness of the c-TiO_2 a Dektak Veeco 150 profilometer was used; the thickness of this layer was measured about 70 nm and verified by SEM image reported in Fig.S5. Patterning of the c-TiO_2 was achieved using a screen printed metal mask which was removed after the c-TiO_2 deposition using an HCl based acidic solution and de-ionized water. A 350 nm nanocrystalline mesoporous m-TiO_2 layer (18NR-T paste, Dyesol, diluted with terpineol and ethyl cellulose) was screen-printed onto the c-TiO_2 surface and successively sintered at 500 °C for 30 min. The perovskite active layer deposition was conducted by double step method; a lead iodide solution (PbI_2 in N,N-dimethylformamide, 460 mg/ml heated at 70°C) was spin coated at 6000 rpm for 10 s and then heated at 80°C for 1h in glove-box environment. $CH_3NH_3PbI_3$ crystallization was achieved by employing the vapor assisted deposition technique proposed by Chen et.al[51] and improved by mean of vacuum environment as extensively reported by Casaluci and co-workers.[52] More in detail, the PbI_2 samples were placed over a hot plate at 150°C for about 1 hour and the methylammonium iodide (MAI) powder was spread around the samples; during this process the samples and the powder were retained under low vacuum (desiccator lid attached to an Edwards 5 E2M5 Rotary Vane Dual Stage Mechanical Vacuum Pump). The complete conversion of PbI_2 layer into $CH_3NH_3PbI_3$ was confirmed by X-EDS analysis reported in Fig.S4.

Finally a solution of 2,20,7,70-tetrakis-(N,N-dip-methoxyphenylamine)9,9'-spirobifluorene (Spiro-MeOTAD, 61.4 mM) doped with tert-butylpyridine(26mM) and Lithium Bis (Trifluoromethanesulfonyl)Imide (Li-TFSI, 55 mM) was spin-coated (2000 rpm for 40 s) in inert atmosphere on perovskite layer. A thickness of about 140 nm for the Spiro-MeOTAD layer was extracted by cross-section SEM image reported in Fig.S5. The final devices were

left in air overnight in a closed box containing silica desiccant prior to realize the gold contacts (100 nm) by mean of high vacuum thermal evaporation.

The GO-Li layer was spin-coated in inert atmosphere (2000 rpm, 60 s) on sintered m-TiO$_2$ layer and then heated @ 80°C for 30 min in air. The GO-Li intercalation into the m-TiO$_2$ was confirmed by Raman spectrum (curve b) reported in Fig.S1. Furthermore the GO-Li deposition over the m-TiO$_2$ has been demonstrated to have a negligible effect into the TiO$_2$ substrate by absorbance measurement reported in Fig. S2. The final devices were not encapsulated.

4.3 Characterizations

The UV-Vis absorption spectra were recorded using UV-Vis 2550 Spectrophotometer from Shimadzu. The spectra were collected over a scan range from 400 to 800 nm at a scan rate of 480 nm/min and a resolution of 1 nm.

Steady-state fluorescence experiments were carried out on a Fluoromax spectrofluorimeter (Jobin-Yvon) operating in the single-photon counting mode.

Raman spectra were acquired by using a Jobin-Yvon-Horiba micro-Raman system (LabRAM ARAMIS) equipped with Ar$^+$ ion laser (514 nm) as the excitation source. The cut-off from the notch filters in the spectrometer is less than 100 cm^{-1}. The laser light reached the sample surface at normal incidence by means of ultra-long working distance (50X) objective with 10.5 mm focal distance. The scattered radiation was collected in a backscattering geometry by a spectrometer equipped with a diffraction grating of 1800 lines/mm coupled to a CCD camera. Spectral de-convolution was carried out by nonlinear least-squares fitting of the Raman peaks to a mixture of Lorentzian and Gaussian line shapes, providing the peak position, width, height, and integrated intensity of each Raman band.

Masked devices were tested in air atmosphere without encapsulation under a solar simulator (ABET Sun 2000, class A) at AM1.5 and 100 mW/cm^2 illumination conditions, calibrated with a certified reference Si Cell (RERA Solutions RR-1002). Incident power was measured whit a Skye SKS 1110 sensor. The class was measured with a BLACK-Comet UV-VIS Spectrometer.

IPCE spectra acquisition were carried out by means of a homemade setup composed by a monochromator (Newport, mod. 74000) coupled with a xenon lamp (Oriel Apex, Newport) and a source meter (Keithley, mod. 2612). A home-made LabVIEW program controls the spectra acquisition.

The measurements involved in the stability test (JV, dark-JV, Transient Photovoltage and Variable Incident Power) were performed with a customized PXI (National Instruments) based platform (ARKEO). The apparatus is composed by an high speed 4 channel source-meter with remote sensing (NI PXIe 4141) and a programmable power supply (NI PXIe 4112) used to drive a high power white led (Bridgelux-50C10K0 @ 5000 Kelvin). Equivalent incident power of 1 SUN (100mW/cm^2) was calibrated through the Mismatch Factor with a certified reference Si Cell (RERA Solutions RR-1002).

The thicknesses of the constituent layers and the EDX profiles were evaluated from Cross-sectional Scanning Electron Microscopy micrographs (FE-SEM Leo Supra 35) equipped with a INCAx-Sight-Oxford Instruments X-EDS.

Acknowledgements

References

[1]   D. Liu, T. L. Kelly, *Nat. Photonics* **2013**, *8*, 133.

[2]   NREL (accessed 2015).

[3]   M. Saliba, K. W. Tan, H. Sai, D. T. Moore, T. Scott, W. Zhang, L. A. Estro, U. Wiesner, H. J. Snaith, *J. Phys. Chem. Lett.* **2014**, *118*, 17171.

[4]   A. Kojima, K. Teshima, Y. Shirai, T. Miyasaka, *J. Am. Chem. Soc.* **2009**, *131*, 6050.

[5]   N. Park, *J. Phys. Chem. Lett.* **2013**, *4*, 2423.

[6]   H.-S. Kim, C.-R. Lee, J.-H. Im, K.-B. Lee, T. Moehl, A. Marchioro, S.-J. Moon, R. Humphry-Baker, J.-H. Yum, J. E. Moser, M. Grätzel, N.-G. Park, *Sci. Rep.* **2012**, *2*, 591.

[7]   K. Wojciechowski, M. Saliba, T. Leijtens, A. Abate, H. J. Snaith, *Energy Environ. Sci.* **2014**, *7*, 1142.

[8]   J. Burschka, N. Pellet, S.-J. Moon, R. Humphry-Baker, P. Gao, M. K. Nazeeruddin, M. Grätzel, *Nature* **2013**, *499*, 316.

[9]   W.-J. Yin, J.-H. Yang, J. Kang, Y. Yan, S.-H. Wei, *J. Mater. Chem. A* **2015**, *3*, 8926.

[10]   G. Xing, N. Mathews, S. Sun, S. S. Lim, Y. M. Lam, M. Grätzel, S. Mhaisalkar, T. C. Sum, *Science* **2013**, *342*, 344.

[11]   A. Abrusci, S. D. Stranks, P. Docampo, H.-L. Yip, A. K.-Y. Jen, H. J. Snaith, *Nano Lett.* **2013**, *13*, 3124.

[12]   J. T. Wang, J. M. Ball, E. M. Barea, A. Abate, J. A. Alexander-webber, J. Huang, M. Saliba, I. Mora-sero, J. Bisquert, H. J. Snaith, R. J. Nicolas, *Nano Lett.* **2014**, *14*, 724.

[13]   W. Zhang, M. Saliba, S. D. Stranks, Y. Sun, X. Shi, U. Wiesner, H. J. Snaith, *Nano Lett.* **2013**, *13*, 4505.

[14]   E. Singh, H. S. Nalwa, *J. Nanosci. Nanotechnol.* **2015**, *15*, 6237.

[15]   E. Singh, H. S. Nalwa, *RSC Adv.* **2015**, *5*, 73575.

[16]   Z. Zhu, J. Ma, Z. Wang, C. Mu, Z. Fan, L. Du, Y. Bai, L. Fan, H. Yan, D. L. Phillips, S. Yang, *J. Am. Chem. Soc.* **2014**, *136*, 3760.

[17]   G. Kakavelakis, D. Konios, E. Stratakis, E. Kymakis, *Chem. Mater.* **2014**, *26*, 5988.

[18]   W. E. Y. Land, *Phys. Rev. B* **1966**, *4*, 4234.

[19]   M. Grätzel, *Nature* **2001**, *414*, 338.

[20]   I. Chung, B. Lee, J. He, R. P. H. Chang, M. G. Kanatzidis, *Nature* **2012**, *485*, 486.

[21] V. Likodimos, T. Stergiopoulos, P. Falaras, R. Harikisun, J. Desilvestro, G. Tulloch, *J. Phys. Chem. C* **2009**, *113*, 9412.

[22] A. Agresti, S. Pescetelli, A. Quatela, S. Mastroianni, T. M. Brown, A. Reale, C. A. Bignozzi, S.Caramori, A. Di Carlo, *RSC Adv.* **2014**, *4*, 12366.

[23] A. Agresti, S. Pescetelli, E. Gatto, M. Venanzi, A. Di Carlo, *J. Power Source* **2015**, *287*, 87.

[24] D. O. Scanlon, C. W. Dunnill, J. Buckeridge, S. Shevlin, A. J. Logsdail, S. M. Woodley, C. R. Catlow, M. J. Powell, R. G. Palgrave, I. P. Parkin, G. W. Watson, T. W. Keal, P. Sherwood, A. Walsh, A. Sokol, *Nat. Mater.* **2013**, *12*, 798.

[25] L. Liu, S. Ryu, M. R. Tomasik, E. Stolyarova, N. Jung, M. S. Hybertsen, M. L. Steigerwald, L. E. Brus, G. W. Flynn, *Nano Lett.* **2008**, *8*, 1965.

[26] D. Kostiuk, M. Bodik, P. Siffalovic, M. Jergel, Y. Halahovets, M. Hodas, M. Omastova, *J. Raman Spectrosc.* **2015**.

[27] A. Das, S. Pisana, B. Chakraborty, S. Piscanec, S. K. Saha, U. V Waghmare, K. S. Novoselov, H. R. Krishnamurthy, A. K. Geim, A. C. Ferrari, A. K. Sood, *Nat. Nanotechnol.* **2008**, *3*, 1.

[28] P. Schulz, E. Edri, S. Kirmayer, G. Hodes, D. Cahen, A. Kahn, *Energy Environ. Sci.* **2014**, *7*, 1377.

[29] Q. Yu, Y. Wang, Z. Yi, N. Zu, J. Zhang, M. Zhang, P. Wang, *ACS Nano* **2010**, *4*, 6032.

[30] S.-J. Park, J.-P. Lee, J. S. Jang, H. Rhu, H. Yu, B. Y. You, C. S. Kim, K. J. Kim, Y. J. Cho, S. Baik, W. Lee, *Nanotechnology* **2013**, *24*, 295202.

[31] G.-J. H. Wetzelaer, M. Scheepers, A. M. Sempere, C. Momblona, J. Ávila, H. J. Bolink, *Adv. Mater.* **2015**, *27*, 1837.

[32] C.-T. Sah, R. N. Noyce, W. Shockleyt, *Proc. IRE* **1956**, *1*, 1228.

[33] G. H. Wetzelaer, M. Kuik, H. T. Nicolai, P. W. M. Blom, *Phys. Rev. B* **2011**, *83*, 165204.

[34] S. D. Stranks, V. M. Burlakov, T. Leijtens, J. M. Ball, A. Goriely, H. J. Snaith, *Phys. Rev. Appl.* **2014**, *2*, 034007.

[35] K. Schwanitz, U. Weiler, R. Hunger, T. Mayer, W. Jaegermann, *J, Phys. Chem. C* **2007**, *111*, 849.

[36] K. Schwanitz, E. Mankel, R. Hunger, T. Mayer, W. Jaegermann, *Chim. Int. J. Chem.* **2007**, *61*, 796.

[37] I. Nakamura, N. Negishi, S. Kutsuna, T. Ihara, *J. Mol. Catal. A Chem.* **2000**, *161*, 205.

[38] T. Leijtens, G. E. Eperon, S. Pathak, A. Abate, M. M. Lee, H. J. Snaith, *Nat. Commun.* **2013**, *4*, 2885.

[39] H. J. Jeong, H. Y. Kim, H. Jeong, J. T. Han, S. Y. Jeong, K.-J. Baeg, M. S. Jeong, G.-W. Lee, *Small* **2014**, *10*, 2057.

[40] R. S. Sanchez, V. Gonzalez-Pedro, J. Lee, N. Park, Y. S. Kang, I. Mora-sero, J. Bisquert, *J. Phys. Chem. Lett.* **2014**, *5*, 2357.

[41] H. Kim, N. Park, *J. Phys. Chem. Lett.* **2014**, *5*, 2927.

[42] H. J. Snaith, A. Abate, J. M. Ball, G. E. Eperon, T. Leijtens, N. K. Noel, S. D. Stranks, J. T. Wang, K. Wojciechowski, W. Zhang, *J. Phys. Chem. Lett.* **2014**, *5*, 1511.

[43] S. van Reenen, M. Kemerink, H. J. Snaith, *J. Phys. Chem. Lett.* **2015**, *6*, 3808.

[44] A. Kongkanand, K. Tvrdy, K. Takechi, M. Kuno, P. V Kamat, *J. Am. Chem. Soc.* **2008**, *130*, 4007.

[45] J. You, Z. Hong, Y. M. Yang, Q. Chen, M. Cai, T. Song, C. Chen, *ACS Nano* **2014**, *8*, 1674.

[46] A. Agresti, S. Pescetelli, S. Casaluci, R. Lettieri, M. Venanzi, A. Di Carlo, In *presented at IEEE-NANO 2015, Rome - Italy (July,2015)*.

[47] W. Tressl, N. Marinoval, O. Inganäs, M. K. Nazeeruddin, S. M. Zakeeruddinl, M. Graetzell, *Photovolt. Spec. Conf. (PVSC), 2014 IEEE 40th* **2014**, 1563.

[48] Z. Hawash, L. K. Ono, S. R. Raga, M. V. Lee, Y. Qi, *Chem. Mater.* **2015**, *27*, 562.

[49] H. L. Poh, F. Šaněk, A. Ambrosi, G. Zhao, Z. Sofer, M. Pumera, *Nanoscale* **2012**, *4*, 3515.

[50] J. Liu, Y. Xue, Y. Gao, D. Yu, M. Durstock, L. Dai, *Adv. Mater.* **2012**, *24*, 2228.

[51] Q. Chen, H. Zhou, Z. Hong, S. Luo, H. Duan, H. Wang, Y. Liu, G. Li, Y. Yang, *J. Am. Chem. Soc.* **2013**, *136*, 622.

[52] S. Casaluci, L. Cinà, A. Pockett, P. S. Kubiak, R. G. Niemann, A. Reale, A. Di Carlo, P. J. Cameron, *J. Power Sources* **2015**, *297*, 504.

Supporting Information
Supporting Information is available from the Wiley Online Library or from the author.

Lithium-Neutralized Graphene Oxide (GO-Li) is inserted for the first time as Electron-Transporting Layer (ETL) in perovskite solar cells (PSC). The proposed device conjugates the extraordinary conduction properties of graphene based materials with the exceptional harvesting behaviour of organoleadtrihalide compounds and shows enhanced power conversion efficiency (PCE) and improved long term stability under operative conditions.

Keywords: Hybrid Organic–Inorganic Perovskite Solar Cells, Lithium-Neutralized Graphene Oxide, Electron Transport Materials (ETM), Photovoltaic Devices.

Antonio Agresti, Sara Pescetelli, Lucio Cinà, Dimitrios Konios, George Kakavelakis, Emmanuel Kymakis, and Aldo Di Carlo[*]

Efficiency and Stability enhancement in Perovskite Solar Cells by inserting Lithium-Neutralized Graphene Oxide as Electron-Transporting Layer.